Fast Calculation of Abort Return Trajectories for Manned Missions to the Moon

Juan S. Senent*

Odyssey Space Research, Houston, TX, 77058, USA

In order to support the anytime abort requirements of a manned mission to the Moon, the vehicle abort capabilities for the translunar and circumlunar phases of the mission must be studied. Depending on the location of the abort maneuver, the maximum return time to Earth and the available propellant, two different kinds of return trajectories can be calculated: direct and fly-by. This paper presents a new method to compute these return trajectories in a deterministic and fast way without using numerical optimizers. Since no simplifications of the gravity model are required, the resulting trajectories are very accurate and can be used for both mission design and operations. This technique has been extensively used to evaluate the abort capabilities of the Orion/Altair vehicles in the Constellation program for the translunar phase of the mission.

I. Introduction

ABORT return trajectories play an important role in the performance of a vehicle designed for manned missions. For a given nominal mission, different abort scenarios can be presented. In this paper, we will cover those scenarios related to the on-orbit performance part and only for Earth to Moon transfers. The main goal will be to calculate abort return trajectories, given the vehicle state and some Entry Interface (EI) constraints, in a fast and accurate way. In order to evaluate the performance of the vehicle, abort trajectories will have to be calculated along the nominal trajectory at different times. In Figure 1, we can see two different abort scenarios for a typical manned mission to the Moon: (a) the abort maneuver is implemented before the Lunar-Orbit-Insertion maneuver (LOI) and (b) the abort maneuver is implemented after a failed LOI. In both cases two strategies can be implemented: a direct return and a Moon flyby. Choosing a direct or flyby return will depend on the abort scenario, distance to the Moon and operational constraints.

In this paper, a method to compute high-fidelity feasible solutions to the abort return problem is described. The first part of the paper summarizes the two techniques used to compute the return trajectories: Pseudostate theory developed by S. Wilson[5,7] and the optimal EI targeter developed by this author.[4] The second part discusses how to integrate these two techniques to calculate abort return trajectories in the translunar and circumlunar phases for the direct and fly-by cases. A discussion about the optimality of the obtained return trajectories, when different entry interface constraints are present, is also included. Finally, some numerical examples and comparisons to the results obtained by numerical optimization are described.

II. Pseudostate theory review

In this section, a brief description of the main results and algorithms of Pseudostate Theory (PT) for Earth-Moon transfers is presented. For a complete explanation of PT and its applications see Refs.[5,7]. In general, in PT a three-body trajectory is approximated by two osculating conics at the beginning and at the end of the propagation (see Figure 2). For the abort problem we are trying to solve, we have an initial state around the Moon and a final state at the Earth EI:

$$\text{initial state (Moon-centered inertial coordinate frame): } t_I, \mathbf{r}_I, \mathbf{v}_I$$
$$\text{final state (Earth-centered inertial coordinate frame): } t_{EI}, \mathbf{R}_{EI}, \mathbf{V}_{EI}$$

*Senior Engineer, Aeroscience and Flight Mechanics Division EG5, Johnson Space Center, 2101 NASA Parkway, Houston, TX, 77058. AIAA Member

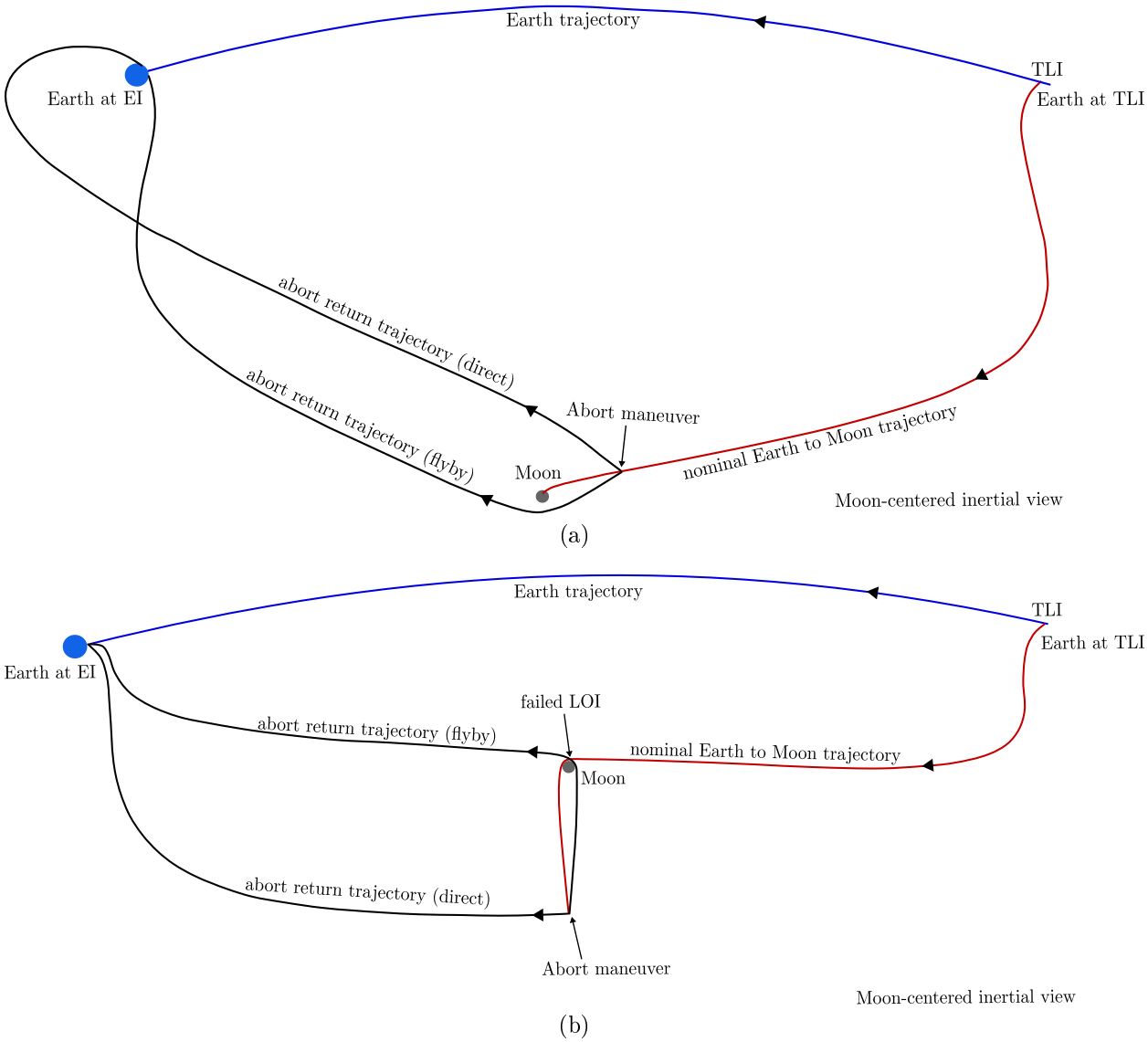

Figure 1. Abort trajectory scenario examples for cases: (a) pre-lunar-orbit-insertion abort and (b) post-lunar-orbit-insertion abort. Nominal Earth to Moon trajectory (red), abort return trajectories (black) and Earth trajectory (blue).

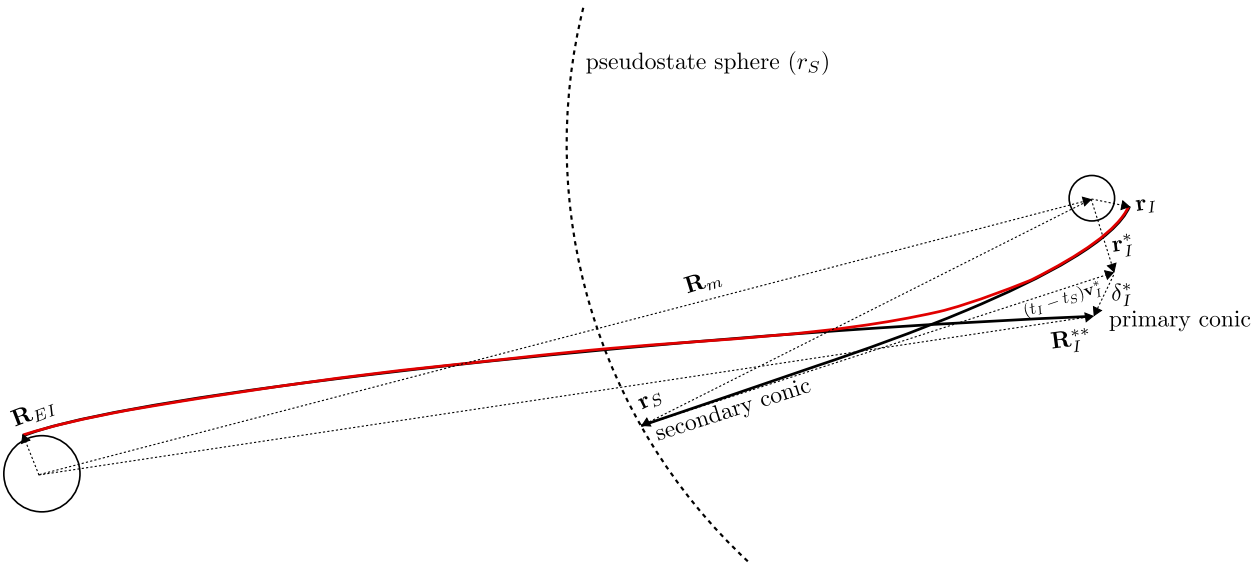

Figure 2. Pseudostate propagation for Earth-Moon transfers. Actual trajectory (red). Primary and secondary conics (solid black).

The goal is to obtain an approximation of the EI state resulting from the propagation of the initial state under the actual gravitational field (function **Propagate**):

$$(\mathbf{R}_{EI}, \mathbf{V}_{EI}) = \mathbf{Propagate}\,(\mathbf{r}_I,\, \mathbf{v}_I,\, t_I,\, t_{EI})$$

The two osculating conics at the above points are:

$$\text{secondary conic: } (t_S, \mathbf{r}_S, \mathbf{v}_S) = \mathbf{Conic2distance}\,(\mathbf{r}_I,\, \mathbf{v}_I,\, r_S,\, \mu_I) \quad (1)$$

$$\text{primary conic: } (\mathbf{R}_{EI}, \mathbf{V}_{EI}) = \mathbf{Conic}\,(\mathbf{R}_I^{**},\, \mathbf{V}_I^{**},\, t_{EI} - t_I,\, \mu_E) \quad (2)$$

The secondary conic propagates the initial Moon-centered inertial state to a distance r_S (function **Conic2distance**) using the gravitational constant μ_I. This distance r_S is defined by the pseudostate sphere radius. For an Earth-Moon transfer r_S is about 24 times the radius of the Earth. From the propagation of the secondary conic we obtain $(t_S, \mathbf{r}_S, \mathbf{v}_S)$, the time and state where the trajectory pierces the pseudostate sphere. The primary conic propagates the primary Earth-centered pseudostate $(t_I,\, \mathbf{R}_I^{**},\, \mathbf{V}_I^{**})$ up to the EI point (function **Conic**) using the gravitational constant μ_E. These two conics are related through two pseudostates: secondary $(\mathbf{r}_I^*, \mathbf{v}_I^*)$ and primary $(\mathbf{R}_I^{**},\, \mathbf{V}_I^{**})$ by

$$\mathbf{v}_I^* = \mathbf{v}_S \quad (3)$$

$$\mathbf{r}_I^* = \mathbf{r}_S + (t_I - t_S)\,\mathbf{v}_S \quad (4)$$

$$\mathbf{R}_I^{**} = \mathbf{R}_m + \mathbf{r}_I^* + \boldsymbol{\delta}_I^* \quad (5)$$

$$\mathbf{V}_I^{**} = \mathbf{V}_m + \mathbf{v}_I^* + \dot{\boldsymbol{\delta}}_I^* \quad (6)$$

where:

$(\mathbf{R}_m, \mathbf{V}_m)$: Moon position and velocity at t_I in Earth-centered inertial coordinates

$\left(\boldsymbol{\delta}_I^*, \dot{\boldsymbol{\delta}}_I^*\right)$: calibration vectors. To take into account high-order gravitational fields and third-body perturbations (e.g. from the SUN).

The propagation process is as follows:

1. Use Eq. 1 to obtain $(t_S, \mathbf{r}_S, \mathbf{v}_S)$.

2. Use Eqs. 3, 4, 5 and 6 to obtain the two pseudostates: $(\mathbf{r}_I^*, \mathbf{v}_I^*)$ and $(\mathbf{R}_I^{**}, \mathbf{V}_I^{**})$

3. Use Eq. 2 to obtain $(\mathbf{R}_{EI}, \mathbf{V}_{EI})$

Note that for propagation-only purposes, no calibration is performed and therefore: $\boldsymbol{\delta}_I^* = \dot{\boldsymbol{\delta}}_I^* = 0$.

A. Three-body Lambert problem

We can modify the propagation algorithm described in the previous section to define a three-body targeting algorithm. Given an initial position and time relative to the secondary body $(t_I, \mathbf{r}_I)$ and a final postion relative to the primary body $(t_E, \mathbf{R}_E)$, we need to calculate the initial and final velocities $(\mathbf{v}_I, \mathbf{V}_E)$. We also need to know the gravitational constants associated with the primary μ_E and secondary μ_I bodies together with the size of the pseudostate sphere associated with the secondary body r_S. In Algorithm 1, we can see a pseudocode version of the proposed procedure. Initially, the secondary pseudostate position and the two calibration vectors are set to zero (line 1 in the algorithm). After that, the pseudostate loop is executed (lines 2 to 15). This loop can be divided into two parts: pseudostate propagation (lines 3 to 9) and calibration (lines 10 to 14).

In line 3, the current estimate of the primary pseudostate position vector is computed from the Moon position at the initial time, the secondary pseudostate and the calibration position vector. In line 4, the primary conic is calculated by solving the Lambert problem from the primary pseudostate position vector $\mathbf{R}_I^{**}$ to the final Earth position vector $\mathbf{R}_E$ for a transfer time $t_E - t_I$. In line 5, the velocity of the secondary pseudostate is calculated $\mathbf{v}_I^*$. From Eq. (3), this is also the velocity at the end of the secondary conic. In line 6, the secondary conic will be calculated. For that, the INRFV problem will be solved (see section B). Once the secondary conic is calculated, we can now get the position vector of the secondary pseudostate $\mathbf{r}_I^*$ from Eq. (4). Finally, we will iterate until the value of $\mathbf{r}_I^*$ has converged with an specified tolerance (line 9). Once the pseudostate propagation part has converged, the calibration part of the algorithm will be executed (lines 10 to 14). In line 10, a numerical propagation of the initial state: $t_I, \mathbf{r}_I, \mathbf{v}_I$ until time t_E is performed. This numerical propagation will incorporate high-order gravity models, third-body perturbations, etc. In general, it will be performed by one or several calls to ODE solvers. If after numerically propagating the solution, the final state $\mathbf{R}_E^{'}$ is close to the target $\mathbf{R}_E$ within some tolerance, the solution has been found and the algorithm exits (line 11). Otherwise, the primary pseudostate vectors $\mathbf{R}_I^{**}$, $\mathbf{V}_I^{**}$ will be obtained by propagating a conic backward in time from the numerically propagated final state $\mathbf{R}_E^{'}, \mathbf{V}_E^{'}$ (line 12). Using Eqs. (5) and (6), we can now calculate the calibration vectors $\boldsymbol{\delta}_I^*$ and $\dot{\boldsymbol{\delta}}_I^*$ (lines 13 and 14).

B. The INRFV problem

The problem we are trying to solve can be defined as (see Figure 3): given an initial position vector $\mathbf{r}_1$ and final velocity $\mathbf{v}_2$ at some distance r_2, calculate the initial velocity $\mathbf{v}_1$ (for a complete description of the solution to this problem see Ref.[6]). For the abort problem we are solving in this paper, we will assume that $r_2 = r_S$ (pseudostate sphere radius) and $r_2 > r_1$. From Figure 3, we can define the angle between $\mathbf{r}_1$ and $\mathbf{v}_2$ as:

$$\psi = \theta + \beta_2$$

$$\begin{aligned} \cos\psi &= \hat{\mathbf{r}}_1^{\mathsf{T}} \hat{\mathbf{v}}_2 \\ \sin\psi &= \pm\sqrt{1-\cos^2\psi} \end{aligned} \tag{7}$$

This problem requires the solution of a quatic equation:

$$A^2x^4 + 2ABx^3 + \left(B^2 + C - 2A\right)x^2 - 2Bx + 1 - C = 0 \tag{8}$$

where:

$$A = \frac{r_2^2 v_2^2}{\mu r_1}, \;\; B = \left(1 - \frac{r_2 v_2^2}{\mu}\right)\sin\psi, \;\; C = \cos^2\psi, \;\; x = \sin\beta_2$$

We can solve this quartic equation analytically. For this work the routine PA05AD from HSL[2] has been used. The formulation of Eq. (8) introduces extraneous solutions, in order to eliminate them we have used

Algorithm 1 Pseudostate three-body Lambert problem

Given: t_I, t_E, $\mathbf{r}_I$, $\mathbf{R}_E$, r_S, μ_E and μ_I
Obtain: $\mathbf{v}_I$ and $\mathbf{V}_E$

Initialization

$\mathbf{r}_I^* = \boldsymbol{\delta}_I^* = \dot{\boldsymbol{\delta}}_I^* = 0$

Pseudostate loop

do

$\mathbf{R}_I^{**} = \mathbf{R}_m + \mathbf{r}_I^* + \boldsymbol{\delta}_I^*$
$(\mathbf{V}_I^{**}, \mathbf{V}_E) = \mathbf{Lambert}\,(\mathbf{R}_I^{**},\, \mathbf{R}_E,\, t_E - t_I,\, \mu_E)$
$\mathbf{v}_I^* = \mathbf{V}_I^{**} - \mathbf{V}_m - \dot{\boldsymbol{\delta}}_I^*$
$(\mathbf{v}_I,\, \mathbf{r}_S,\, t_S) = \mathbf{INRFV}\,(\mathbf{r}_I,\, \mathbf{v}_I^*,\, r_S,\, \mu_I)$
$\mathbf{r}_I^{*'} = \mathbf{r}_I^*$
$\mathbf{r}_I^* = \mathbf{r}_S + (t_I - t_S)\,\mathbf{v}_I^*$
if $\left|\mathbf{r}_I^* - \mathbf{r}_I^{*'}\right| >$ tolerance **cycle**

Calibration

$\left(\mathbf{R}_E^{'}, \mathbf{V}_E^{'}\right) = \mathbf{Propagate}\,(\mathbf{r}_I,\, \mathbf{v}_I,\, t_I,\, t_E)$
if $\left|\mathbf{R}_E - \mathbf{R}_E^{'}\right| <$ tolerance **exit**
$(\mathbf{R}_I^{**},\, \mathbf{V}_I^{**}) = \mathbf{Conic}\left(\mathbf{R}_E^{'}, \mathbf{V}_E^{'},\, t_I - t_E,\, \mu_E\right)$
$\boldsymbol{\delta}_I^* = \mathbf{R}_I^{**} - \mathbf{R}_m - \mathbf{r}_I^*$
$\dot{\boldsymbol{\delta}}_I^* = \mathbf{V}_I^{**} - \mathbf{V}_m - \mathbf{v}_I^*$

end do

the following criteria (see Ref.[6] for a complete explanation): If $\cos\psi > 0 \Leftrightarrow \mathbf{r}_1^{\mathsf{T}}\mathbf{v}_2 > 0$, $\sin\beta_2$ is the smaller of the real positive solutions. If $\cos\psi < 0 \Leftrightarrow \mathbf{r}_1^{\mathsf{T}}\mathbf{v}_2 < 0$, $\sin\beta_2$ is the larger of the real positive solutions. Once $\sin\beta_2$ has been found we can compute $\mathbf{v}_1$ and $\mathbf{r}_2$ as follows:

$$\begin{aligned} \hat{\mathbf{c}} &= \frac{\hat{\mathbf{r}}_1 \times \hat{\mathbf{v}}_2}{\sin\psi} \\ \theta &= atan2(\sin\psi, \cos\psi) - \sin\beta_2 \\ \mathbf{r}_2 &= r_2\left[\cos\theta\hat{\mathbf{r}}_1 + \sin\theta\,(\hat{\mathbf{c}} \times \hat{\mathbf{r}}_1)\right] \end{aligned} \tag{9}$$

$$v_1 = \sqrt{v_2 - 2\frac{\mu}{r_2} + 2\frac{\mu}{r_1}} \qquad p = \frac{(r_2 v_2 \sin\beta_2)^2}{\mu}$$

$$f = 1 - \frac{r_2\,(1 - cos\theta)}{p} \qquad g = \frac{r_2 r_1 \sin\theta}{\sqrt{\mu p}}$$

$$\mathbf{v}_1 = \frac{\mathbf{r}_2 - f\mathbf{r}_1}{g}$$

One final note about the problem. The sign of $\sin\psi$ can be chosen arbitrarily (see Eq. (7)). Therefore there are two antiparallel choices for the direction of the angular momentum (see Eq. (9)). In one case $\mathbf{r}_1$ will be located after periapse (see Figure 3 solid red line) and in the second case $\mathbf{r}_1$ will be located before periapse (see Figure 3 dashed red line). This is important for the abort problem we are trying to solve because just by changing the direction of the angular momentum we can specify the abort solutions to do a Moon flyby or not (direct return). In Figure 1, we can see that in both scenarios: cases (a) and (b), we can always find a direct and a Moon flyby return.

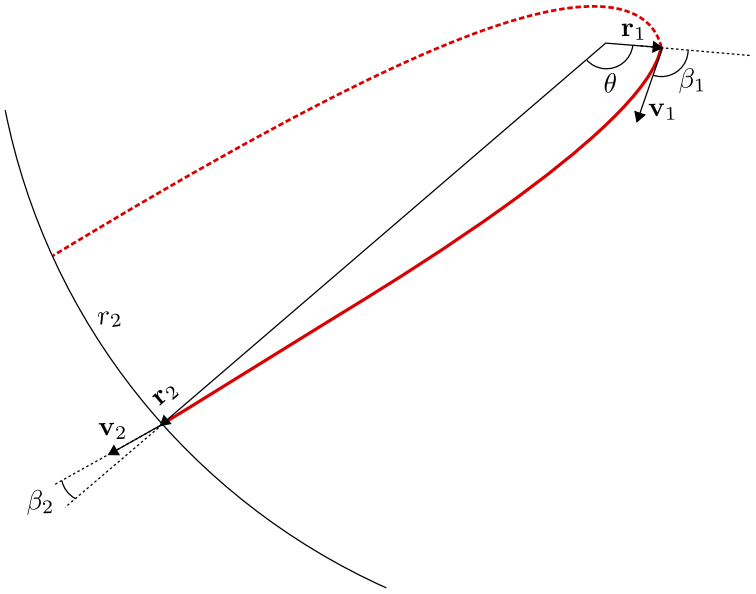

Figure 3. INRFV problem definition. Depending on the sign of $\sin\psi$ two different solutions can be obtained (red solid and red dashed curves).

III. Three-body abort targeting problem

In this section, the three-body problem formulated in Algorithm 1 will be modified so it can be used as a targeting algorithm for abort problems. The main difference between the proposed abort-targeting algorithm and Algorithm 1 is the use of a different method to calculate the primary conic. Instead of using a Lambert arc for this algorithm, an optimal two-body abort targeting algorithm developed by the author[4] will be used. In general, this algorithm will solve the following problem: Given an initial state $(t, \mathbf{R}, \mathbf{V})$, a transfer time Δt to Entry Interface (EI) and a gravitational constant μ, calculate an optimal impulsive maneuver $\mathbf{\Delta V}$ such that at EI the following constraints are satisfied:

equality constraints: r_{EI}, γ_{EI}	EI radius and flight-path-angle.
inequality constraints: λ_{EI}, L_{EI}, Az_{EI}	EI longitude, latitude and azimuth.

As described in Ref.[4], this targeting algorithm has some properties that makes it suitable for the problem we are trying to solve in this paper. In general, the algorithm is non-iterative (an iteration procedure is used when the EI velocity with respect to the Δt is calculated but this is done only once) and it provides a global optimal solution and feasibility information about the problem.

The three-body abort targeting algorithm (see Algorithm 2) is very similar to the one in Algorithm 1. Therefore, only the differences between them will be described. Whereas the Lambert routine only needs the position vectors at the beginning and at the end of the arc, the optimal abort algorithm described in this section will need a complete state at the initial time and some constraints at EI. In order to compute the full primary pseudostate (t_I, $\mathbf{R}_I^{**}$, $\mathbf{V}_I^{**}$) , the secondary pseudostate will have to be defined first. In line 2 of Algorithm 2, the secondary pseudostate is initialized and in line 6, the primary pseudostate velocity is calculated. In lines 7 and 8, the primary conic is calculated such that it satisfies the EI constraits specified: r_{EI}, γ_{EI} at the least or r_{EI}, γ_{EI} and some inequality constraints on λ_{EI}, L_{EI}, Az_{EI}. The computation of the primary conic and the calibration section of the algorithm (from line 9 to 19) are identical to the ones in Algorithm 1. One final difference between both targeting algorithms is that as Algorithm 2 converges to the solution $\Delta V_I^{**} \to 0$, whereas previously only $\left|\mathbf{r}_I^* - \mathbf{r}_I^{*'}\right| \to 0$ and $\left|\mathbf{R}_{EI} - \mathbf{R}_{EI}^{'}\right| \to 0$. Finally, the initialization of the secondary pseudostate $\mathbf{r}_I^*, \mathbf{v}_I^*$ in lines 1 and 2 is not unique. Through numerical tests it was shown that $\mathbf{r}_I^* = 0$, $\mathbf{v}_I^* = \mathbf{v}_I$ performs well in the type of problems solved in this paper. It is also worth mentioning that as suggested in Ref.[5], the use of a pre-periapse pseudostate instead of using always the post-periapse one (as in Algorithm 2) can reduce the number of iterations. In numerical results we have

Algorithm 2 Three-body abort targeting problem

Given: t_I, t_{EI}, $\mathbf{r}_I$, $\mathbf{v}_I$, r_{EI}, γ_{EI}, r_S, μ_E and μ_I
Obtain: $\mathbf{\Delta v}_I$ and EI conditions

Initialization

$\mathbf{r}_I^* = 0$
$\mathbf{v}_I^* = \mathbf{v}_I$
$\boldsymbol{\delta}_I^* = \dot{\boldsymbol{\delta}}_I^* = 0$

Pseudostate loop

do

$\mathbf{R}_I^{**} = \mathbf{R}_m + \mathbf{r}_I^* + \boldsymbol{\delta}_I^*$
$\mathbf{V}_I^{**} = \mathbf{V}_m + \mathbf{v}_I^* + \dot{\boldsymbol{\delta}}_I^*$
$(\mathbf{\Delta V}_I^{**}, \mathbf{R}_{EI}, \mathbf{V}_{EI}) = \mathbf{Abort}\left(\mathbf{R}_I^{**}, \mathbf{V}_I^{**}, r_{EI}, \gamma_{EI}, t_{EI} - t_I, \mu_E\right)$
$\mathbf{V}_I^{**} \leftarrow \mathbf{V}_I^{**} + \mathbf{\Delta V}_I^{**}$
$\mathbf{v}_I^* = \mathbf{V}_I^{**} - \mathbf{V}_m - \dot{\boldsymbol{\delta}}_I^*$
$\left(\mathbf{v}_I^{'}, \mathbf{r}_S, t_S\right) = \mathbf{INRFV}\left(\mathbf{r}_I, \mathbf{v}_I^*, r_S, \mu_I\right)$
$\mathbf{r}_I^{*'} = \mathbf{r}_I^*$
$\mathbf{r}_I^* = \mathbf{r}_S + (t_I - t_S)\,\mathbf{v}_I^*$
if $\left|\mathbf{r}_I^* - \mathbf{r}_I^{*'}\right| >$ tolerance **cycle**

Calibration

$\left(\mathbf{R}_{EI}^{'}, \mathbf{V}_{EI}^{'}\right) = \mathbf{Propagate}\left(\mathbf{r}_I, \mathbf{v}_I, t_I, t_{EI}\right)$
if $\left|\mathbf{R}_{EI} - \mathbf{R}_{EI}^{'}\right| <$ tolerance **exit**
$\left(\mathbf{R}_I^{**}, \mathbf{V}_I^{**}\right) = \mathbf{Conic}\left(\mathbf{R}_{EI}^{'}, \mathbf{V}_{EI}^{'}, t_I - t_{EI}, \mu_E\right)$
$\boldsymbol{\delta}_I^* = \mathbf{R}_I^{**} - \mathbf{R}_m - \mathbf{r}_I^*$
$\dot{\boldsymbol{\delta}}_I^* = \mathbf{V}_I^{**} - \mathbf{V}_m - \mathbf{v}_I^*$

end do
$\mathbf{\Delta v}_I = \mathbf{v}_I^{'} - \mathbf{v}_I$

seen that the pre-periapse pseudostate reduces the number of iterations in cases where the trajectory is just entering the pseudostate sphere. Once the trajectory is inside the pseudostate sphere both pseudostates (pre and post-periapse) perform similarly for the cases evaluated in this work.

IV. Optimality of the solutions

In this section, we will discuss the optimality of the solutions for the three-body and two-body targeting algorithms described above. The three-body version of the algorithm, which includes calls to the two-body algorithm, will be used when the pseudostate conditions apply. That is when the vehicle is inside the pseudostate sphere. Otherwise, the two-body version will be used. One difference in the performance of both algorithms is that the three-body version will generate high-fidelity solutions. Since the three-body version incorporates a calibration phase where actual trajectories are calculated, the final answer is always a return trajectory numerically integrated with high-order gravity fields, third-body perturbation, central-body switching, etc. The two-body version does not contain any calibration and only two-body equations are used. Therefore no high-fidelity trajectory is obtained.

A. Optimality of the optimal two-body abort targeting algorithm

When the vehicle is located outside the pseudostate sphere, the optimal two-body abort algorithm will be used (see line 7 in Algorithm 2 and also in Ref.[4]). In this section, we will compare the Δv associated with the abort maneuvers obtained with the two-body version of the algorithm to the ones obtained using a numerical optimizer. The index used for the performance evaluation of the targeter is:

$$\text{relative error} = 100\frac{|\Delta \mathbf{v}_{tar} - \Delta \mathbf{v}^*|}{\Delta v^*}$$

where $\Delta \mathbf{v}_{tar}$ is the solution obtained using the two-body targeting algorithm and $\Delta \mathbf{v}^*$ is the solution obtained by the numerical optimizer.

The numerically optimized solution will be computed taking into account high-order gravity models, perturbations, etc. The gravity model used in all the examples consists of an 8x8 Earth and includes the Moon and the Sun as point masses. The Copernicus[1,3] trajectory optimization tool has been used to numerically optimize the initial guess provided by the targeter. For a given nominal trajectory, different impulsive abort maneuvers are calculated for different Abort Times (AT) and Return Times (RT). AT is the time elapsed from the Trans-Lunar-Injection maneuver (TLI) to the abort maneuver time. RT is the time elapsed from the abort maneuver time to EI. As for the EI constraints, two cases are considered: (a) equality constraints in the EI radius and flight-path angle and (b) same as in case (a) plus inequality constraints in the EI azimuth. In Figure 4, we can see that the relative error between the actual Δv and the one calculated by the targeting algorithm is always less than 1% for the cases examined. Whereas the relative error increases when RT increases (this is due to the fact that the trajectory is affected by third-body perturbations as RT increases), the relative error due to different ATs is not as relevant as the one produced by changing RT. This is due to the fact that the Δv magnitude decreases when AT increases (the vehicle is getting further from the Earth) and therefore the relative error remain the same, although the absolute error increases. In Figure 4 we can see the magnitude of the initial position vector for different ATs. Given the two-body nature of the algorithm, it is expected that its performance deteriorates with this distance (i.e. when ATs increases).

When comparing both cases in Figure 4, we can also see that in case (b) the relative error between different ATs is closer than in case (a). Adding the azimuth constraint reduces the number of possible solutions and therefore the trajectories obtained by the two-body targeter and the numerical optimizer are closer.

The computational time for this routine is 0.11 ms in average. Given that the routine is mainly analytical, adding more constraints to the problem does not substantially increase the computational time.

B. Optimality of the optimal three-body abort targeting algorithm

As in the previous section, the optimality of the three-body version of the algorithm has been tested against numerically optimized solutions. For a given nominal trajectory to the Moon, several ATs and RTs have been evaluated. The process consisted of generating a feasible solution for several ATs and RTs by Algorithm 2 and use this solution as the initial guess for the numerically optimized trajectory. The trajectory is propagated using two different segments centered at the Moon and at the Earth. The gravity model used for the computation of the solutions is:

- Moon-centered segment: 8x8 Moon, Earth and Sun point masses.
- Earth-centered segment: 8x8 Earth, Moon and Sun point masses.

The performance is evaluated based on three parameters: relative and absolute error in Δv and CPU factor:

$$\begin{aligned} \text{relative error} &= 100\frac{\Delta v_{tar} - \Delta v^*}{\Delta v^*} \\ \text{absolute error} &= \Delta v_{tar} - \Delta v^* \\ \text{CPU factor} &= \frac{CPUtime_{optimizer}}{CPUtime_{pseudostate}} \end{aligned}$$

where Δv_{tar} and Δv^* are defined as in the previous section, $CPUtime_{optimizer}$ is the time it takes for Copernicus to find the optimal solution (the overhead associated with Copernicus initialization is not included) and $CPUtime_{pseudostate}$ is the time it takes for Algorithm 2 to find the solution.

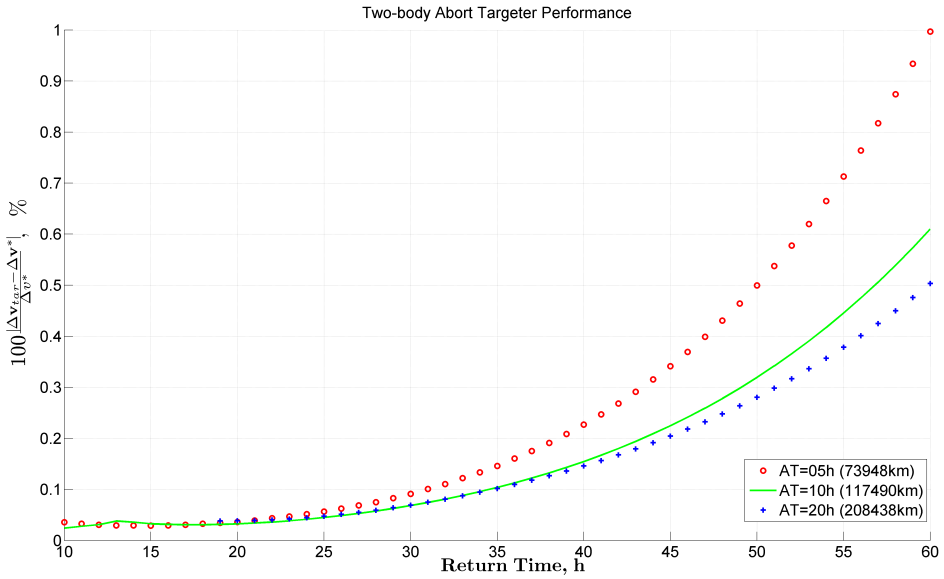

(a)

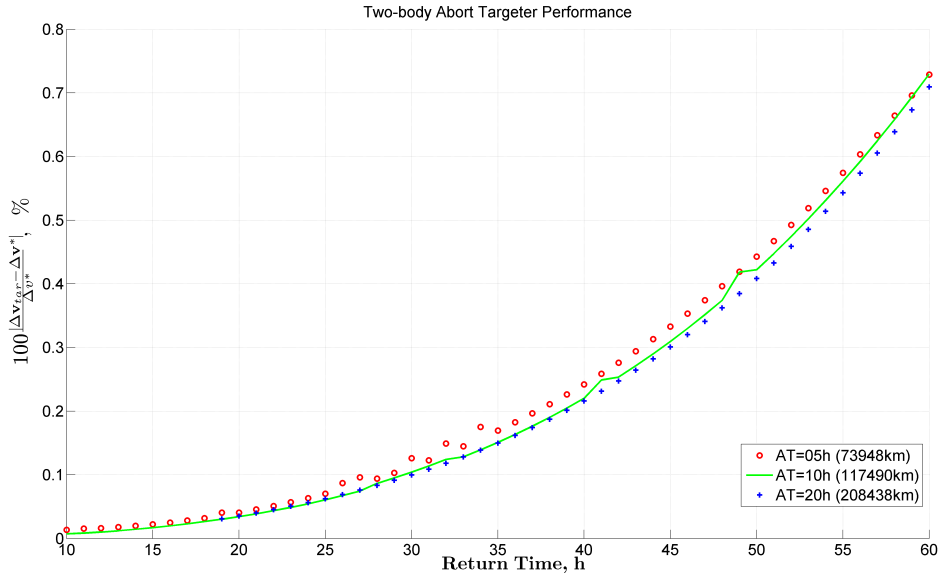

(b)

Figure 4. Comparison between the high-fidelity numerically optimized solution and the two-body solution for three different ATs and several RTs. The results are expressed in error Δv percentage. (a) EI radius and flight-path angle equality constraints. (b) EI radius, flight-path angle equality constraints and inequality constraints in the EI azimuth $[30°, 60°]$.

A summary of the test cases evaluated is in Table 1. This table also shows the CPU times associated with Algorithm 2 for each of the test cases. We can use the CPU time in this table together with the CPU factor presented in all the figures (for example, see Figure 5) to compute the average CPU time associated with the numerically optimized solution.

From the results in Figures 5, 6 and 7, we can conclude that the trajectories generated by Algorithm 2 are simply feasible trajectories. Although, the calculation of the primary conic is done in an optimal way, this does not guarantee the optimality of the solution. The maximum deviation in Δv found in the examples is about 20% for flyby cases and 6% for direct return cases. But the time it takes for the optimizer to find the solution is several times the time it takes for Algorithm 2 (see Figures 5, 6 and 7 to examine specific cases).

It is interesting to note that when the number of constraints in the problem increases (reducing the number of possible trajectories) the solutions obtained by Algorithm 2 are closer to the ones obtained by the optimizer. A similar effect was shown in the previous case for the two-body version of the abort targeter. As an example, when the EI Azimuth is constrained as in cases 5 and 6 in Table 1, the maximum relative error is reduced to less than 2% (see Figure 7). In Table 1, we can also see that adding constraints to Algorithm 2 does not affect substantially the CPU time. This is due to the fact that all the EI constraints are handled in the computation of the primary conic and this is done analytically in a process with no iterations.

Table 1. 3-Body Targeter (Algorithm 2) Computational Time Performance

Case	$ALTD_{EI}$	γ_{EI}	Az_{EI}	Flyby		AT=65h	AT=75h	AT=85h
1	✓	✓	✗	✗	mean	0.34 s	0.19 s	0.18s
					std	0.27 s	0.05 s	0.03 s
2	✓	✓	✗	✓	mean	0.23 s	0.15 s	0.16 s
					std	0.03 s	0.01 s	0.01 s
3	✓	✓	[30°, 60°]	✗	mean	0.20 s	0.19 s	0.18 s
					std	0.07 s	0.07 s	0.06 s
4	✓	✓	[30°, 60°]	✓	mean	0.31 s	0.17 s	0.17 s
					std	0.03 s	0.015 s	0.01 s
5	✓	✓	[44°, 46°]	✗	mean	0.2 s	0.19 s	0.19 s
					std	0.07 s	0.06 s	0.05 s
6	✓	✓	[44°, 46°]	✓	mean	0.29 s	0.18 s	0.18 s
					std	0.03 s	0.02 s	0.01 s

V. Conclusions

Generating an optimal abort return trajectory for Earth to Moon transfers can be computationally expensive when considering realistic EI constraints and high-order gravity models at the Earth and Moon together with third-body perturbations. The use of an initial guess generator can reduce substantially the computational time. In this paper, a two-body and three-body abort targeting algorithms have been presented. They can both be used as initial guess generators for numerical optimizers. We have shown that their computational time is several orders of magnitude less than the ones associated with numerical optimizers. We have also discussed the optimality of the solutions found by both targeters. We have concluded that whereas the two-body version of the targeter produces solutions close to the optimal (even for cases not close to the Earth), the three-body version of the algorithm generates only good feasible solutions. Depending on how constrained the problem is, those solutions can be very close to the optimal too (see Figure 7). The main advantages of the proposed algorithms are:

- They can produce feasible solutions in a reasonable amount of time: 0.11 ms for the two-body version and 0.5s for the three-body version. It is worth mentioning that the three-body version incorporates calibration, which increases the computational time but at the same time allows the generation of high-fidelity feasible solutions (including realistic EI constraints and gravity fields).

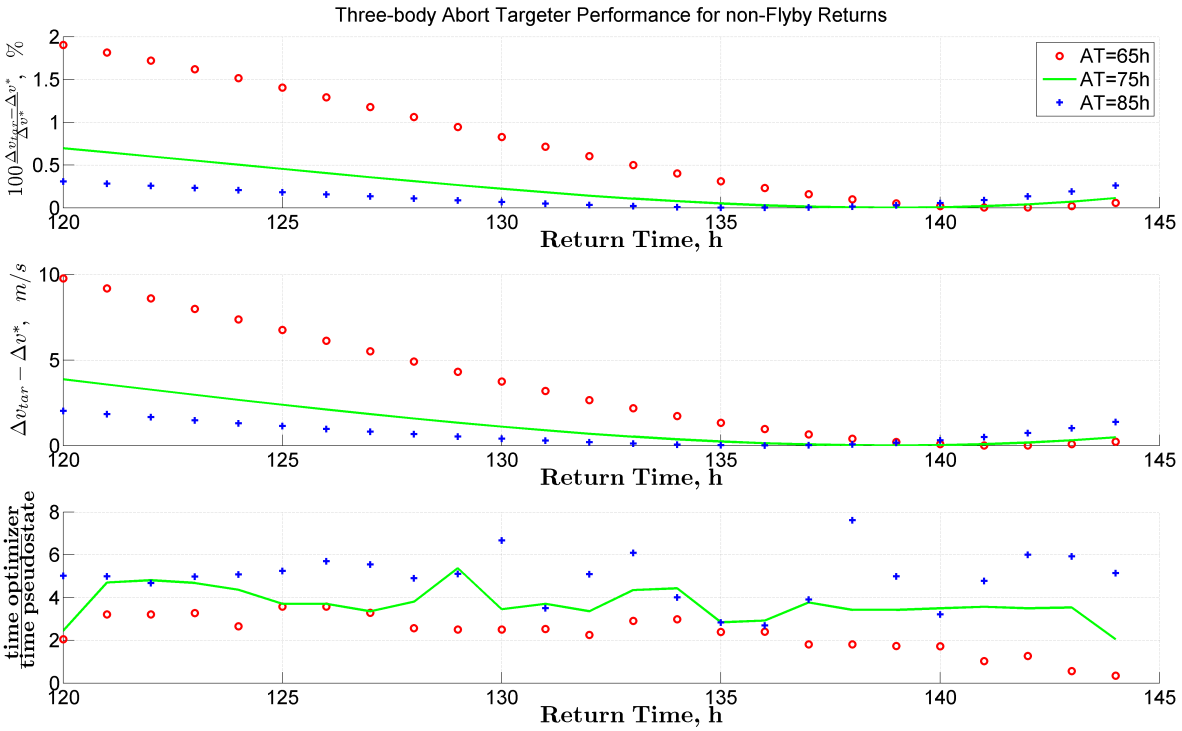

(a)

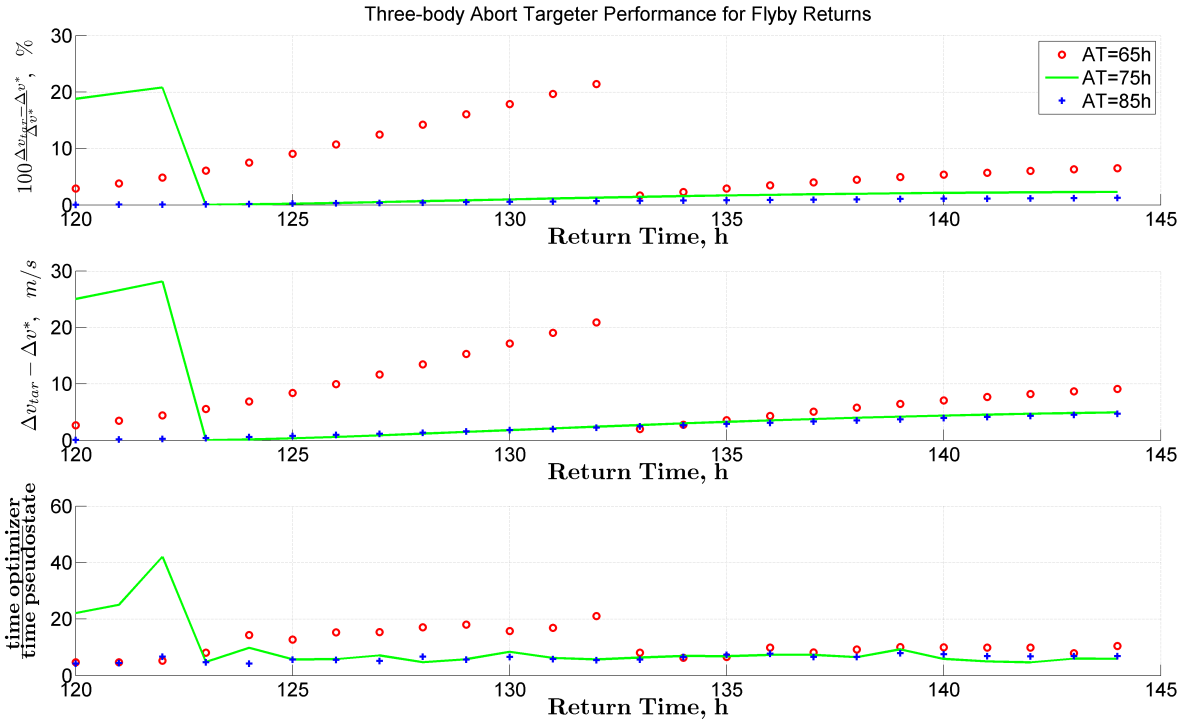

(b)

Figure 5. Performance evaluation of the Three-body targeter for Cases 1 (top) and 2 (bottom) in Table 1.

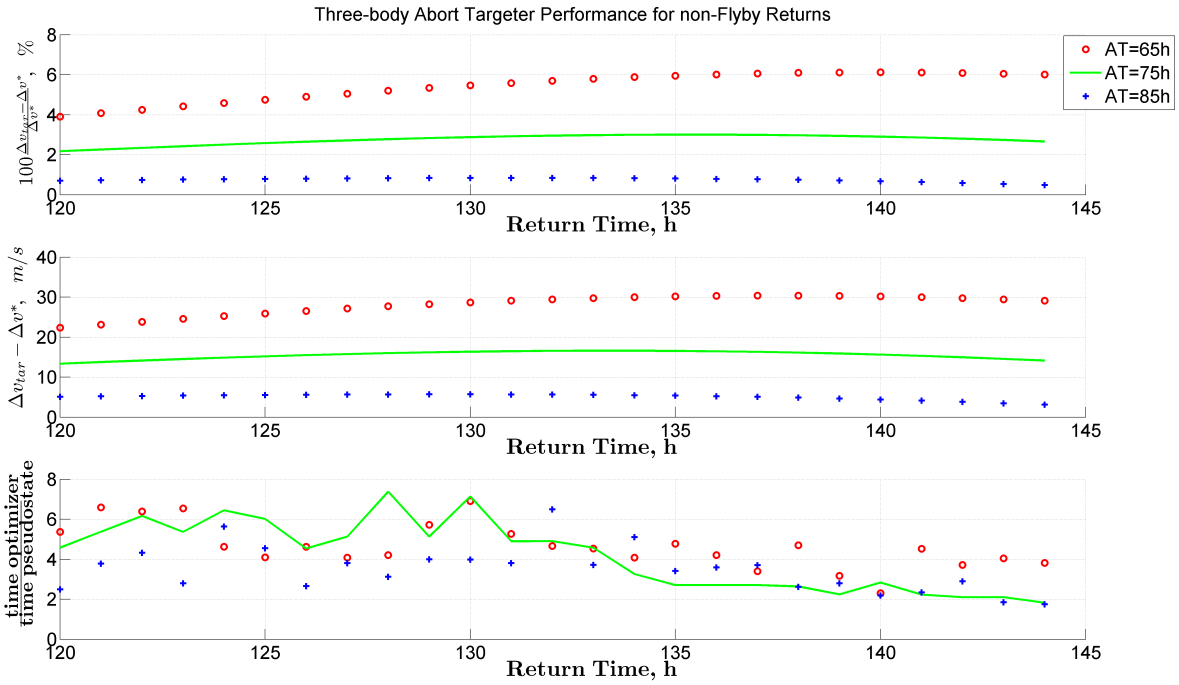

(a)

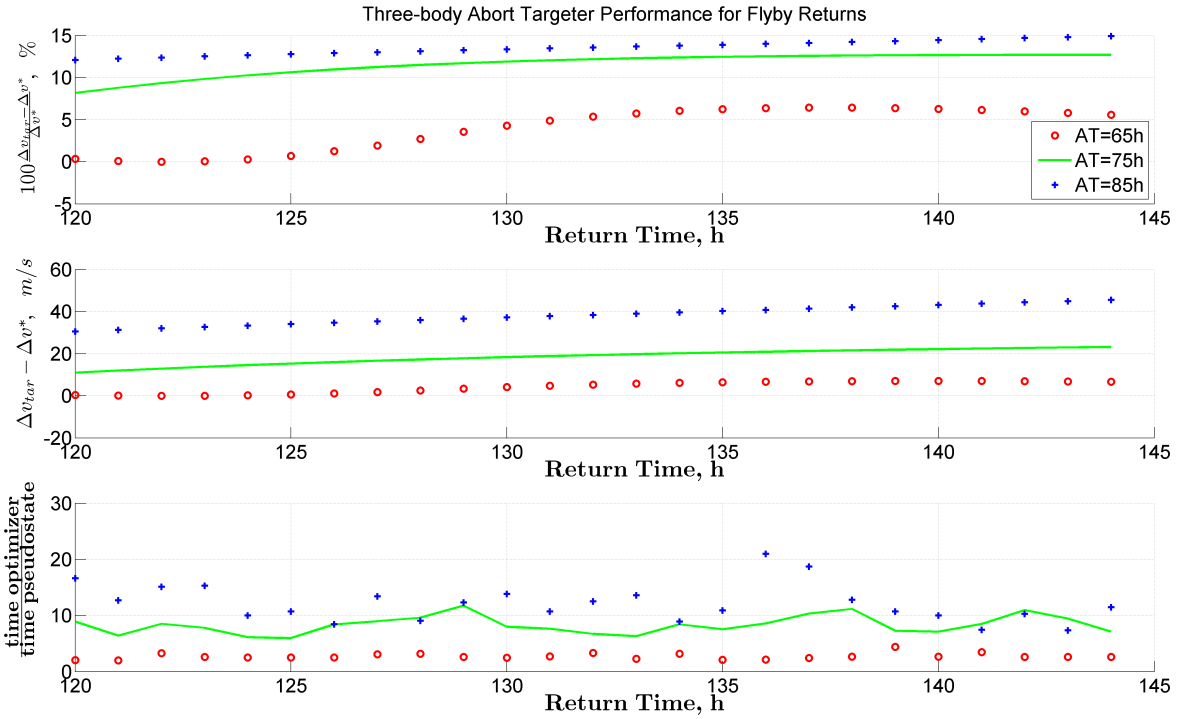

(b)

Figure 6. Performance evaluation of the Three-body targeter for Cases 1 (top) and 2 (bottom) in Table 1

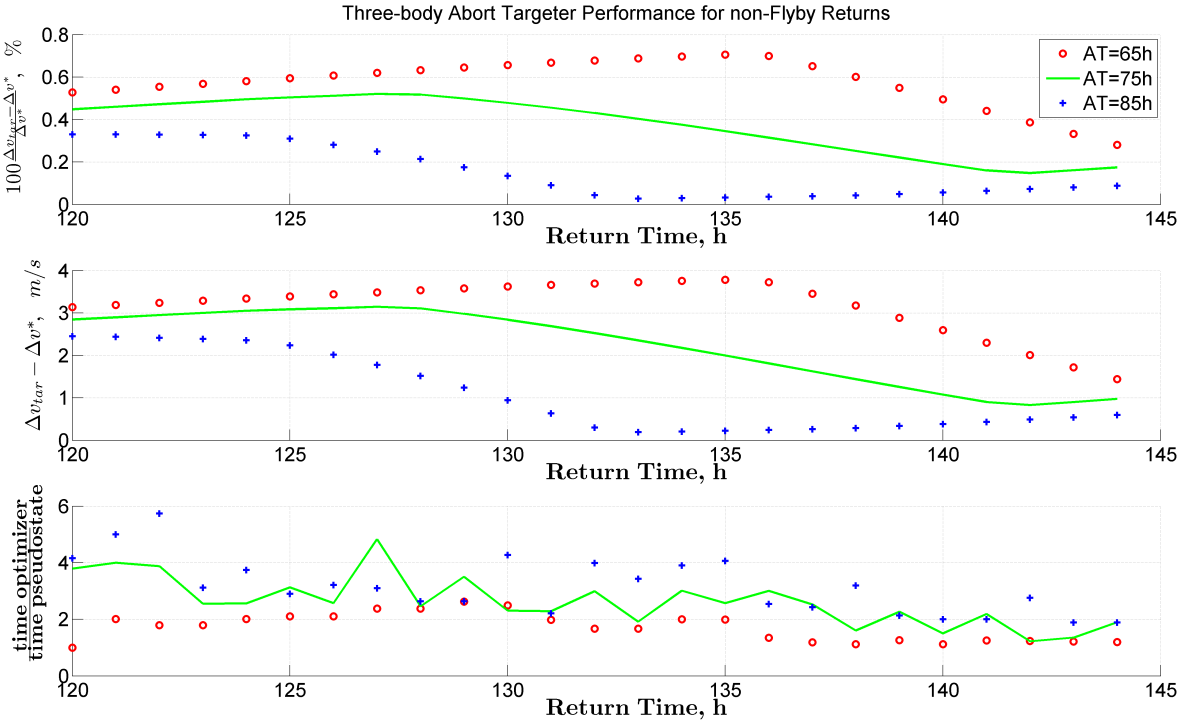

(a)

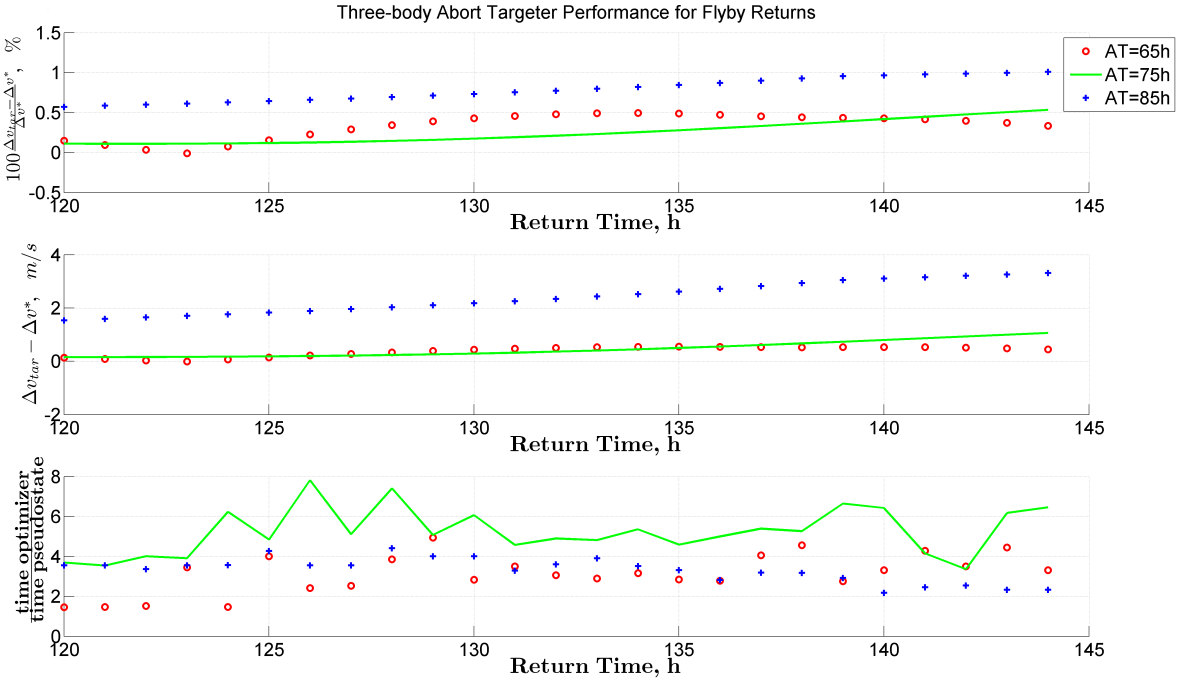

(b)

Figure 7. Performance evaluation of the Three-body targeter for Cases 1 (top) and 2 (bottom) in Table 1

- The type of solution (flyby or direct) can be specified. Whereas numerical optimizers might pick the optimal one of the two approaches, these algorithms allow the user to evaluate a specific one.
- They can be easily modified to solve some similar one-impulse return trajectory problems. Although not shown in this paper, Algorithm 2 has been also used to calculate one-impulse trans-Earth-injection, partial-TLI and partial-LOI abort return trajectories with similar performance to the one described above. Hardly no modifications were needed to handle these additional problems.

Acknowledgments

The author would like to thank J. Williams and J. Gutkowski from the On-orbit Performance Group of the Aeroscience and Flight Mechanics division at the Johnson Space Center for their very constructive comments and suggestions.

References

[1]Ocampo C., Senent J.S., and Williams J. Theoretical Foundation of Copernicus: A Unified System for Trajectory Design and Optimization. In *4th International Conference on Astrodynamics Tools and Techniques. Madrid, Spain.*, May 2010.

[2]The Numerical Analysis Group. Pa05ad. HSL archive a catalogue of subroutines, January 1994. http://hsl.rl.ac.uk/archive/hslarchive.html.

[3]Williams J., Senent J.S., Ocampo C., Mathur R., and Davis E. C. Overview and Software Architecture of the Copernicus Trajectory Design and Optimization System. In *4th International Conference on Astrodynamics Tools and Techniques. Madrid, Spain.*, May 2010.

[4]Senent J.S. An Optimal Initial Guess Generator for Entry Interface Targeters. In *Proceedings of the 2009 AAS/AIAA Astrodynamics Specialist Conference. Pittsburgh. Pennsylvania.*, number AAS 09-426, 2009.

[5]Wilson S. W. A Pseudostate Theory for the Approximation of Three-Body Trajectories. Technical Report MSC/TRW Task A-60.1, Mission Planning and Analysis Division NASA Manned Spacecraft Center, 1969.

[6]Wilson S. W. Physical Identification of the Extraneous Roots Obtained During Solution of the INRFV Problem. Technical Report MSC/TRW Task A-237, Mission Operations Analysis Department. TRW Systems Group, Feb 1970.

[7]Wilson S. W. Investigation of Recursive Pseudostate Iteration Procedures for Solving Split Boundary Value Problems Associated with Interplanetary Trajectories. Technical Report MSC/TRW Task A-516, Mission Operations Analysis Department. TRW Systems Group, May 1971.